Article

# A bio-inspired O$_2$-tolerant catalytic CO$_2$ reduction electrode

Xu Lu [a,b], Zhan Jiang [c], Xiaolei Yuan [a,b,d], Yueshen Wu [a,b], Richard Malpass-Evans [e], Yiren Zhong [a,b], Yongye Liang [c,*], Neil B. McKeown [e,*], Hailiang Wang [a,b,*]

[a] Department of Chemistry, Yale University, New Haven, CT 06520, USA
[b] Energy Sciences Institute, Yale University, West Haven, CT 06516, USA
[c] Department of Materials Science and Engineering, Shenzhen Key Laboratory of Printed Organic Electronics, Southern University of Science and Technology, Shenzhen 518055, China
[d] Institute of Functional Nano and Soft Materials, Jiangsu Key Laboratory for Carbon-Based Functional Materials and Devices, Soochow University, Suzhou 215123, China
[e] EastChem, School of Chemistry, University of Edinburgh, Edinburgh EH9 3FJ, UK

ABSTRACT

The electrochemical reduction of CO$_2$ to give CO in the presence of O$_2$ would allow the direct valorization of flue gases from fossil fuel combustion and of CO$_2$ captured from air. However, it is a challenging task because O$_2$ reduction is thermodynamically favored over that of CO$_2$. 5% O$_2$ in CO$_2$ near catalyst surface is sufficient to completely inhibit the CO$_2$ reduction reaction. Here we report an O$_2$-tolerant catalytic CO$_2$ reduction electrode inspired by part of the natural photosynthesis unit. The electrode comprises of heterogenized cobalt phthalocyanine molecules serving as the cathode catalyst with >95% Faradaic efficiency (FE) for CO$_2$ reduction to CO coated with a polymer of intrinsic microporosity that works as a CO$_2$-selective layer with a CO$_2$/O$_2$ selectivity of ~20. Integrated into a flow electrolytic cell, the hybrid electrode operating with a CO$_2$ feed gas containing 5% O$_2$ exhibits a FE$_{CO}$ of 75.9% with a total current density of 27.3 mA/cm$^2$ at a cell voltage of 3.1 V. A FE$_{CO}$ of 49.7% can be retained when the O$_2$ fraction increases to 20%. Stable operation for 18 h is demonstrated. The electrochemical performance and O$_2$ tolerance can be further enhanced by introducing cyano and nitro substituents to the phthalocyanine ligand.

© 2019 Science China Press. Published by Elsevier B.V. and Science China Press. All rights reserved.

## 1. Introduction

Electrochemical reduction of CO$_2$ to useful chemicals would contribute to solving the greenhouse gas issue and to utilizing renewable energy [1–10]. For such an artificial photosynthesis process to be viable, the feed gas should come from a practical CO$_2$ source such as fossil fuel flue gases or gases from direct air capture systems, both of which contain a significant amount of O$_2$. For example, a typical exhaust gas generated by combustion of fossil fuels has an O$_2$/CO$_2$ ratio of ~20% [11], whereas CO$_2$ captured and concentrated from air by a moisture-swing sorption method is expected to contain up to 10% O$_2$ [12,13]. The presence of O$_2$ poses a tangible threat to the reduction reaction of CO$_2$. Thermodynamically, O$_2$ has a reduction potential more than 1 V higher than that of CO$_2$ and, kinetically, CO$_2$ reduction often demands a larger overpotential compared to O$_2$ reduction [14,15]. These effects combine to ensure that CO$_2$ is strongly unfavored to compete for electrons with O$_2$. The current mainstream solution is to purify CO$_2$

before feeding it to an electrolyzer, which requires an additional gas separation system and extra energy input [16,17]. Nature does it differently. The plant photosynthesis process employs enzymes near the reactive sites to increase the local CO$_2$ concentration to up to 1,000 times the atmospheric level [18,19]. With the lowered O$_2$/CO$_2$ ratio, CO$_2$ can be efficiently converted to glucose at a fast rate in spite of the competing O$_2$-reduction photorespiration process [20]. This biological strategy provided the inspiration for the design of an artificial electrode within which CO$_2$ can be enriched to facilitate its reduction in the presence of O$_2$.

Herein, we report a catalytic electrode that can selectively produce CO by reducing CO$_2$ in a feed gas containing a significant percentage of O$_2$. The electrode design integrates three components: (1) a CO$_2$ concentrator, (2) a gas diffusion electrode (GDE), and (3) a catalyst layer. The CO$_2$ concentrator is composed of a thin layer of a polymer of intrinsic microporosity (PIM), which can impede O$_2$ transport but is highly permeable to CO$_2$. The catalyst is cobalt phthalocyanine (CoPc) molecules anchored on carbon nanotubes (CNTs). Integrated into a flow electrolyzer, the PIM-CoPc/CNT hybrid electrode affords effective and durable CO$_2$ reduction with substantially improved O$_2$ tolerance. With 5% O$_2$ in the CO$_2$ feed gas, a Faradaic efficiency for CO production (FE$_{CO}$)

of 75.9% with a total geometric current density ($j_{total}$) of 27.3 mA/cm$^2$ is achieved at a cell voltage of 3.1 V. The electrode can retain a $FE_{CO}$ of 49.7% and a $j_{total}$ of 28.6 mA/cm$^2$ when the O$_2$ volume fraction increases to 20%. Adjusting the substituents on the Pc ligand of the supported molecular catalyst allows us to further improve the O$_2$ tolerance and electrochemical performance. Since the competition between CO$_2$ reduction and O$_2$ reduction is a function of the O$_2$/CO$_2$ ratio at the catalytic sites, based on the experimentally observed dependence, we deduce that the PIM layer has a CO$_2$/O$_2$ selectivity of 16.5–23.5. Without the CO$_2$ concentrating layer, the CoPc/CNT electrode essentially cannot perform CO$_2$ reduction at all when the feed gas contains 5% of O$_2$.

## 2. Materials and methods

### 2.1. Synthesis of catalyst materials

All chemicals were purchased from commercial sources and used as received unless otherwise noted. All aqueous solutions were prepared with deionized water (Millipore 18.2 MΩ cm).

The synthesis of CoPc-CN was based on a reported method with some modifications [21]. Typically, 1,2,4,5-tetracyanobenzene (8.4 mmol, 1.5 g) and cobalt(II) acetate tetrahydrate (2.6 mmol, 0.65 g) were well mixed in 25 mL of tetramethylene sulfone with ten drops of 1,8-diazabicyclo[5.4.0]undec-7-ene in a seal tube. Subsequently, the tube was filled with Ar, sealed, and kept at 145 °C for 5 h. The reaction mixture was then dispersed in 200 mL of methanol and the resulting precipitate was collected, washed with ether and dried in vacuum. The solid was further purified by Soxhlet extraction with methanol, after which it was dissolved in N,N′-dimethylformamide (DMF) and filtered. The solution was evaporated in vacuum to afford the target compound as a dark-green solid (0.34 g, 21%). UV–Vis: $\lambda_{max}$ (DMF) 686.4 nm; HRMS (ESI) calculated for CoC$_{40}$H$_8$N$_{16}$: 771.04553, found: 771.04470.

To synthesize CoPc-NO$_2$, 4-nitrophthalonitrile (10 mmol, 1.73 g), cobalt(II) chloride hexahydrate (CoCl$_2$·6H$_2$O, 2.5 mmol, 0.60 g), urea (80 mmol, 4.80 g) and a catalytic amount of ammonium molybdate were first ground into a homogeneous mixture in an agate mortar. Then, the mixture was reacted in the solid state at 170 °C for 5 h under Ar atmosphere. The resulting product was stirred at 90 °C for 1 h in HCl (1 mol/L, 200 mL) and then in NaOH (1 mol/L, 200 mL). The solid was filtered, washed with water and dried in vacuum. The crude product was purified by Soxhlet extraction with methanol. The resulting product was then dissolved in DMF and filtered. The DMF solution was evaporated under vacuum to afford the CoPc-NO$_2$ compound as a dark-green solid (0.83 g, 44%). UV–Vis: $\lambda_{max}$ (DMF) 675.3 nm; HRMS (ESI) calculated for CoC$_{32}$H$_{12}$N$_{12}$O$_8$: 751.02385, found: 751.02344.

To synthesize CoPc-NH$_2$, CoPc-NO$_2$ (1.5 g, 2 mmol), sodium sulfide nonahydrate (Na$_2$S·9H$_2$O, 9.6 g, 40 mmol), 2 mL of deionized water and 50 mL of DMF were mixed in a three-necked round-bottom flask, and the mixture was stirred at 60 °C overnight under Ar atmosphere. After that, the solution was evaporated under vacuum, and the obtained solid was washed with water and then boiled in a 200 mL 5 wt% aqueous sodium hydroxide solution. Subsequently, the precipitate was filtered and washed with water. The resulting solid was poured into 500 mL of water with stirring, and 1 mol/L HCl was added to adjust the pH to 5. Filtration was applied to remove undissolved side products. The pH of the filtered solution was then adjusted to 8 by adding 1 mol/L KOH and the resulting solution was boiled. The formed precipitate was collected by filtration, washed with water and methanol, and dried in vacuum to afford the target CoPc-NH$_2$ compound as a dark-green solid (1.03 g, 82%). UV–Vis: $\lambda_{max}$ (DMF) 705.0 nm; HRMS (ESI) calculated for CoC$_{32}$H$_{20}$N$_{12}$: 631.12604, found: 631.12435.

CoPc, CoPc-CN, CoPc-NO$_2$ and CoPc-NH$_2$ molecules were anchored onto multi-wall carbon nanotubes (CNTs) (CNano Technology Ltd.) based on our previous work [22]. The CNTs were first calcined at 500 °C in air for 5 h. After cooling down to room temperature, the CNTs were transferred into a 5 wt% HCl aqueous solution and sonicated for 30 min. The purified CNTs were collected by filtration and washed with deionized water thoroughly. 30 mg of the purified CNTs were dispersed in 30 mL of DMF by sonication for 1 h. Then, a calculated amount of CoPc, CoPc-CN, CoPc-NO$_2$ or CoPc-NH$_2$ dissolved in DMF was added to the CNT suspension and then sonicated for 30 min to obtain a well-mixed suspension. The suspension was further stirred at room temperature for 20 h. The mixture was then centrifuged and the precipitate was washed with DMF and ethanol. Finally, the precipitate was lyophilized to yield the final product. The cobalt content in the hybrid materials was adjusted to be ∼0.27 wt%.

CoO$_x$/CNT was prepared following a previous work [23]. 4 mg of mildly-oxidized CNTs were dispersed in 14 mL of ethanol and sonicated for 1 h. 0.8 mL of Co(CH$_3$COO)$_2$·4H$_2$O aqueous solution (0.2 mol/L) and 0.8 mL of NH$_3$·H$_2$O (28.0 wt%–30.0 wt%) were added to the suspension in sequence. The mixture was kept at 80 °C in an oil bath for 12 h for the reaction to complete. After centrifuging and washing with deionized water for three times, the product was lyophilized and stored under ambient conditions.

### 2.2. Synthesis of PIM

The preparation of PIM was based on a previous work [24]. A mixture of 3,3,3′,3′-tetramethyl-1,1′-spirobisindane-5,5′,6,6′-tetrol (5.0000 g, 14.69 mmol), 2,3,5,6 tetrafluorophthalonitrile (2.9389 g, 14.69 mmol, recrystallized from ethanol) and anhydrous potassium carbonate (16.2390 g, 117.50 mmol) in 100 mL of anhydrous dimethylformamide was stirred at 65–70 °C for 72 h. The bright yellow mixture was cooled to room temperature, poured into 500 mL of water and stirred for 1 h. The solid was collected by filtration, washed with deionized water and then acetone until the washings were clear. The resulting powder was dried and dissolved in tetrahydrofuran. Subsequently, methanol was added drop-wise until the solution became turbid. The solution was further stirred for 30 min to precipitate a gel. The polymer was then dissolved in tetrahydrofuran and added drop-wise to a 500 mL mixture of methanol and acetone (1:1) with vigorous stirring and the precipitated fine powder was filtered. The powder was refluxed in methanol for 24 h, filtered and then dried in a vacuum oven at 120 °C for 9 h to afford the desired polymer (6.65 g, 92%) as a bright yellow powder. $\nu_{max}$ (polymer film) (cm$^{-1}$): 2,953, 2,864, 2,241, 1,445, 1,262, 1,009; $^1$H NMR (250 MHz, CDCl$_3$): $\delta_H$ = 6.81 (br, s, 2H, Ar H), 6.42 (br, s, 2H, Ar H), 1.56 (br, m, 4H, 2 CH$_2$), 1.31 (br, m, 12H, 4 CH$_3$); GPC (Chloroform): $M_n$ = 60,400, $M_w$ = 194,700. BET surface area = 812 m$^2$/g; total pore volume = 0.7648 cm$^3$/g at $P/P_o$ = 0.9814; TGA analysis (polymer film): initial weight loss due to thermal degradation commences at ∼500 °C with a 87% loss of mass below 1,000 °C.

### 2.3. Gas selectivity measurement in pressure increase apparatus

Polymer membranes were prepared by casting a PIM solution (2 wt%–5 wt% in tetrahydrofuran) into a flat-bottomed glass dish. The solvent was evaporated slowly under a slow flow of N$_2$ at ambient temperature to give a bright yellow membrane. CO$_2$/O$_2$ selectivity of the as-prepared polymer membrane was deduced from gas permeation data, which were measured at 30 °C with pure CO$_2$ and O$_2$ gases using a custom-made fixed-volume pressure-increase instrument (typically at 200–300 mbar). Prior to each measurement, the system was sufficiently evacuated to completely remove the previous gas.

## 2.4. Hybrid electrode preparation

10 mg of catalyst powder was dispersed in 5 mL of ethanol, followed by the addition of 40 μL of 5 wt% Nafion perfluorinated resin solution and a bath sonication for 1 h. Then, a calculated amount of the homogeneously mixed ink was deposited on one side of a 0.6 cm × 0.9 cm × 0.37 mm polytetrafluoroethylene-hydrophobized carbon fiber paper (Toray 120, Fuel Cell Store) and dried under an IR lamp. The final loading of the catalyst was 0.37 mg/cm². Then, 15 mg of PIM was dissolved in 3 mL of chloroform. 600 μL of the solution was deposited dropwise on the other side of the carbon fiber paper and dried in a fume hood. The adopted volume was an optimized result (Fig. S1 online).

## 2.5. Flow electrolyzer fabrication

The flow electrolyzer was fabricated following our previously published protocol [25]. The 0.6 cm × 0.9 cm × 0.37 mm anode and cathode were housed between two 0.5 mm thick poly(methyl methacrylate) (PMMA) plates, where a $(0.2 × 0.5)$ cm² window was cut out. Two identical 0.2 mm thick PMMA plates with a 0.2 cm × 7 cm channel were adjacently placed to facilitate the laminar electrolyte flows. An anion exchange membrane (AEM, Selemion DSV) was sandwiched in-between as the separator. A 5 cm × 1 cm × 0.5 cm gas reservoir was constructed on the cathode side to deliver $CO_2/O_2$ feed gas to the opposing-catalyst side of the cathode. The anode is $CoO_x$/CNT coated on a carbon fiber paper electrode with a mass loading of 0.37 mg/cm². A leakage test was carried out prior to each experiment by immersing the electrolyzer into a beaker filled with water and passing Ar gas through all channels.

## 2.6. Electrochemical measurements

The electrochemical measurements were controlled by an electrochemical workstation (Bio-Logic VMP3 Multi Potentiostat). The cell polarization profiles were obtained by the chronoamperometry technique. Each data point was an average over a run time of 180 s. Currents were normalized to the geometric active area of the electrode, i.e., 0.1 cm². We noted that the current density variation from device to device was larger than common H-cell studies because of the much smaller working electrode area. Two 0.5 mol/L $KHCO_3$ aqueous solutions were used as the catholyte and anolyte, which were driven into the flow cell using a dual-channel syringe pump (LSP02-1B, Longer Pump) at a constant flow rate of 0.5 mL/min. After passing through the electrolyzer, the catholyte and gas effluents were combined and collected by a home-made collector. Due to the limitation of our cell design, the cathode potential was estimated by measuring the potential difference between the cathode and an external Ag/AgCl reference electrode immersed in the catholyte effluent, which gave a cathode potential of about −1.1 V vs. RHE at the cell voltage of −3.1 V. When conducting long-term electrolysis, a dual-channel peristaltic pump (P625, Instech) was used to circulate the electrolytes at a constant flow rate of 0.5 mL/min. All the electrolyte solutions were purified before use following a method described in our previous work [26]. To adjust the volume fraction of $O_2$, high-purity $CO_2$ (99.999%, Airgas Inc.) and $O_2$ (99.999%, Airgas Inc.) were mixed in a home-made gas mixer at calculated flow rates as controlled by independent mass flow controllers (Alicat Scientific), and finally delivered to the gas reservoir at a total flow rate of 20 sccm. Gas products were extracted from the home-made collector placed at the outlet of the gas chamber and the catholyte channel for analysis by a GC (SRI Multiple Gas Analyzer #5) equipped with molecular sieve 5A and HayeSep D columns. $N_2$ was used as the carrier gas. $H_2$ and CO were quantified by a thermal conductivity detector (TCD) and a flame ionization detector (FID), respectively. Gas volumes were obtained from the output peak areas using calibration curves. No liquid product was detected in our experiments.

## 3. Results

CO is one of the most cost-effective products from electrochemical $CO_2$ reduction because it could be further electrochemically reduced to hydrocarbons [27,28] or used as a feedstock in the Fischer-Tropsch process to produce liquid fuels [29]. Besides noble metals such as Au and Ag [30,31], metal-nitrogen coordination materials, with our CoPc-based molecules anchored on CNTs as an example [22], are selective and active electrocatalysts for $CO_2$ conversion to CO [32,33]. When CoPc/CNT is used as the cathode catalyst in a flow electrolytic cell that we have recently constructed [25], pure $CO_2$ can be converted to CO with high efficiency. In the voltage range of 2.7–3.7 V, the cell exhibits $FE_{CO} > 93\%$ and $FE_{H_2} < 10\%$, with $j_{total}$ increasing with the voltage from 18.4 to 54.7 mA/cm² (Fig. 1). In sharp contrast, when 5% $O_2$ is incorporated in the $CO_2$ feed gas, $FE_{CO}$ and $FE_{H_2}$ drop drastically to essentially zero in the examined voltage range (Fig. 1), indicating that $O_2$ reduction has already been completely dominant at this relatively low $O_2/CO_2$ ratio. The higher current density in the presence of $O_2$ is likely associated with faster $O_2$ reduction compared with $CO_2$ reduction.

Inspired by plant photosynthesis (Fig. 2a), our design strategy for the $O_2$-tolerant catalytic $CO_2$ reduction electrode is to integrate in the electrode a function of concentrating $CO_2$ from a $CO_2/O_2$ mixture. We chose a PIM material (Fig. S2 online) to serve as a molecular sieve with high gas permeability [24,34]. The size-selective pores within the polymer structure can reject bigger $O_2$ molecules (kinetic diameter = 0.346 nm [35,36]) and allow rapid transport of smaller $CO_2$ molecules (kinetic diameter = 0.33 nm [35,37]). A thick (100 μm) membrane of this polymer demonstrates a $CO_2/O_2$ selectivity of ∼6.2 in a pressure-increase time-lag apparatus [24]. Our electrode adopts a layered architecture, where the CoPc/CNT catalyst and the PIM are coated on opposing sides of a carbon fiber paper GDE (Fig. 2b). It was anticipated that the gas selection layer would lower the $O_2/CO_2$ ratio of the feed gas reaching the supported molecular catalyst so that it can effectively perform $CO_2$-to-CO conversion.

The PIM-CoPc/CNT hybrid electrode was integrated into our flow electrolytic cell (Fig. S3 online) which was operated at a controlled voltage of 3.1 V for maximized $FE_{CO}$ (Fig. S4 online). Without any $O_2$ in the $CO_2$ feed gas, $FE_{CO}$ is 96.9% with $j_{total} = 29.3$ mA/cm² (Fig. 2c), similar to the control without the PIM gas selection layer (Fig. 1). Measurements were then conducted with $O_2$ in the feed gas to assess the $O_2$ tolerance of the electrode. With 5% $O_2$, $CO_2$ reduction to CO can still proceed with a high FE of 75.9% and a total current density of 27.3 mA/cm², indicating effective size-exclusion of $O_2$ by the PIM layer. With stepwise increments of 5% in the $O_2$ content, $j_{total}$ stays at ∼30 mA/cm² and $FE_{H_2}$ remains below 6%, whereas $FE_{CO}$ gradually decreases to 69.7% at 10% $O_2$, 60.6% at 15% $O_2$, 49.7% at 20% $O_2$, 43.3% at 25% $O_2$, and 32.1% at 30% $O_2$ (Fig. 2c). As the volume fraction of $O_2$ increases to 35%, $FE_{CO}$ falls below 20.0% and $j_{total}$ increases to 34.9 mA/cm², suggesting that $O_2$ reduction dominates the electrode reaction. Our $CO_2$ electrolytic cell shows stable performance during long-term operation. With 5% $O_2$ in the $CO_2$ feed gas, $FE_{CO}$ remains largely stable between 79.4% and 75.8% for 18 h of continuous electrolysis at a controlled cell voltage of 3.1 V, with $j_{total} = ∼32$ mA/cm² (Fig. 2d). Good durability is also achieved with a high $O_2$ volume fraction of 20%: Throughout the entire 18 h period, $FE_{CO}$ slowly descends from 53.7% to 48.4% (Fig. 2d).
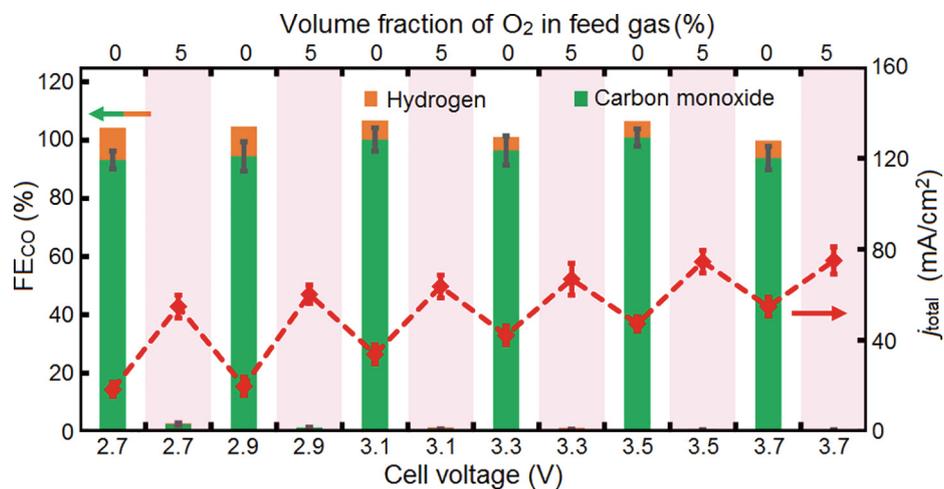
**Fig. 1.** (Color online) $FE_{CO}$, $FE_{H_2}$ and $j_{total}$ vs. cell voltage with and without $O_2$ in the feed gas. CoPc/CNT is used as the cathode catalyst, $CoO_x$/CNT as the anode catalyst, and 0.5 mol/L aqueous $KHCO_3$ as the electrolyte. Error bars represent standard deviations from multiple measurements.
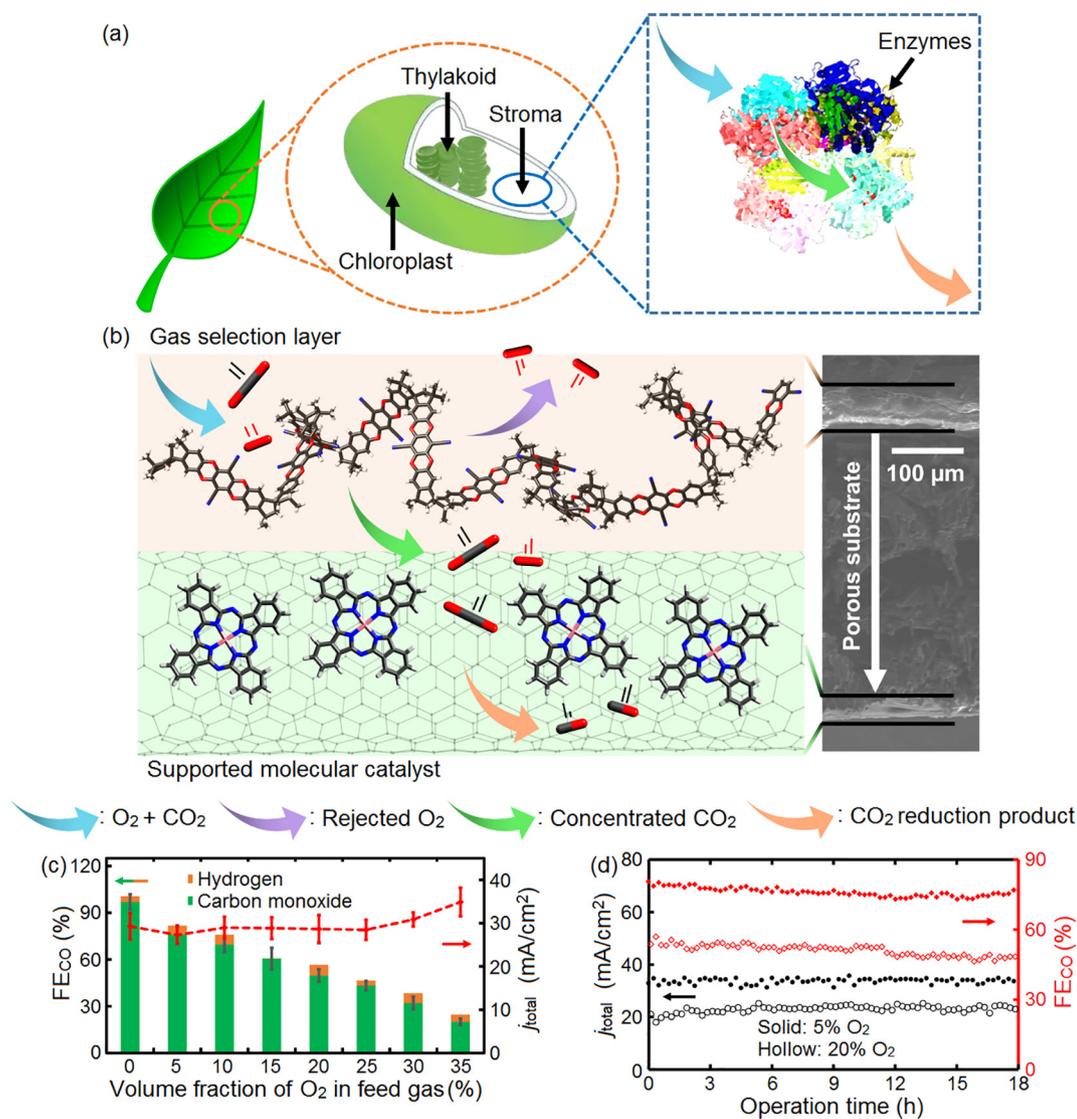


**Fig. 2.** (Color online) Design principle and electrochemical performance. (a) Illustration of plant photosynthesis in the presence of $O_2$. (b) Schematic diagram and cross-section scanning electron microscopy image of the architecture of the PIM-CoPc/CNT hybrid electrode for $O_2$-tolerant catalytic $CO_2$ reduction. Atoms: black, carbon; red, oxygen; pink, cobalt; blue, nitrogen. (c) $FE_{CO}$, $FE_{H_2}$ and $j_{total}$ vs. volume fraction of $O_2$ in the $CO_2$ feed gas. Error bars represent standard deviations from multiple measurements. (d) $FE_{CO}$ and $j_{total}$ during an 18 h electrolysis at $O_2$ volume fractions of 5% (solid markers) and 20% (hollow markers). PIM-CoPc/CNT is used as the cathode, $CoO_x$/CNT as the anode catalyst, and 0.5 mol/L aqueous $KHCO_3$ as the electrolyte. Cell voltage: 3.1 V.

A notable advantage of our molecular CoPc-based catalyst materials is that their catalytic sites can be tailored by chemical synthesis to introduce substituents that might further enhance performance. Our prior work has revealed that electron-withdrawing substituents on CoPc can improve the electrocatalytic activity for $CO_2$ reduction to CO [22]. Hence, we prepared cyano-, nitro- and amino-substituted CoPc molecules (Fig. S5 online) and their corresponding hybrids with CNTs. With pure $CO_2$ as the feed gas, the three hybrid materials can all catalyze $CO_2$ electroreduction with $FE_{CO} > 90\%$ (Fig. S6). With $CO_2$ containing 5% $O_2$, the three substituted CoPc-based electrodes, like CoPc/CNT, all completely lose their function for catalyzing $CO_2$ reduction (Fig. S6 online). However, integrating a PIM $CO_2$-concentrating layer imparts $O_2$ tolerance to all electrodes (Figs. S7 and S8 online). Because ligand modification influences both the catalytic activity for $CO_2$ reduction and that for $O_2$ reduction, $O_2$-tolerant $CO_2$ reduction could be further enhanced. Indeed, the PIM-CoPc-CN/CNT electrode can deliver a $j_{total}$ of 56.3 mA/cm$^2$ with a $FE_{CO}$ of 83.7% at a cell voltage of 3.1 V in the presence of 5% $O_2$ in the $CO_2$ feed gas (Fig. S8a online), demonstrating higher reaction rates and selectivity. The PIM-CoPc-NO$_2$/CNT electrode has even higher $O_2$ tolerance, showing a $FE_{CO+H_2}$ as high as 82.3% in the presence of 20% $O_2$ (Fig. S8b online).

## 4. Discussion

The PIM layer plays a pivotal role in this bio-inspired electrode structure. It filters $O_2$ and enriches $CO_2$ from the feed gas, and thus creates a low-$O_2$ local environment for the catalyst to effectively perform electrochemical $CO_2$ reduction to CO. For a given catalyst, the reaction selectivity between $CO_2$ reduction and $O_2$ reduction should be dependent on the $O_2/CO_2$ ratio at the catalyst surface, if the other conditions are held constant. This allows us to derive the local $O_2/CO_2$ ratio at the catalyst surface of the $O_2$-tolerant hybrid electrodes and to further estimate the $CO_2$ concentrating power of the PIM layer. For each CoPc-based catalyst, we first recorded the dependence of the $FE_{O_2}/FE_{CO}$ ratio on the $O_2/CO_2$ feed ratio in the PIM-free electrode configuration (Fig. S9a–d online), and then compared with the $O_2/CO_2$-dependent $FE_{O_2}/FE_{CO}$ data for the corresponding PIM-containing electrode (Fig. S9e–h and Table S1 online) to determine the local $O_2/CO_2$ ratio at the catalyst surface at each $O_2/CO_2$ feed ratio (Fig. S10 online). The results derived independently from the four different CoPc-based catalysts are consistent and reflect the capability of the PIM layer in selectively transporting $CO_2$ over $O_2$. As the volume fraction of $O_2$ increases from 0 to 35% in the feed gas, the local $O_2$ concentration at the catalyst is maintained below 2%, corresponding to an average $CO_2/O_2$ selectivity of ~20 (Fig. 3), which suggests that ~95% $O_2$ in the feed gas is rejected by the PIM layer. Compared to the $CO_2/O_2$ selectivity of 6.2 measured in the standard pressure-increase apparatus, the enhanced separation in our electrolyzer could be attributed to the gas–liquid co-flow configuration as well as the relatively high concentration of $CO_2$ in the feed gas.

## 5. Conclusions

In summary, we have devised a bio-inspired hybrid electrode structure to realize efficient and durable $O_2$-tolerant electrocatalytic $CO_2$ reduction. This unprecedented performance is based on the cooperation between the microporous polymer that selectively permeate $CO_2$ and the heterogenized molecular catalyst that actively converts $CO_2$ to CO. The reaction rate and $O_2$ tolerance can be further enhanced by appending substituents to the catalyst structure. These electrodes may be useful for directly valorizing
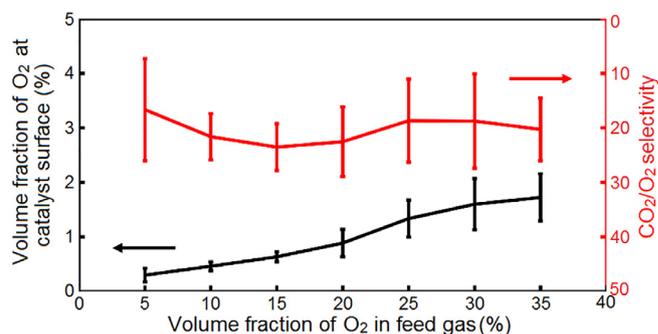


**Fig. 3.** (Color online) Volume fraction of $O_2$ at the catalyst surface vs that in the feed gas, and $CO_2/O_2$ selectivity of the PIM gas selection layer in the $O_2$-tolerant hybrid electrodes. Error bars represent standard deviations from measurements of PIM-CoPc-CN/CNT, PIM-CoPc/CNT, PIM-CoPc-NH$_2$/CNT, and PIM-CoPc-NO$_2$/CNT electrodes as shown in Fig. S10 online.

$O_2$-containing industrial flue gases or utilizing $CO_2$ from direct air capture.

## Conflict of interest

The authors declare that they have no conflict of interest.

## Author contributions

Xu Lu and Hailiang Wang conceived the idea and designed the experiments. Richard Malpass-Evans and Neil B. McKeown provided the PIM. Zhan Jiang and Yongye Liang prepared the catalysts. Xu Lu, Xiaolei Yuan, Yueshen Wu and Yiren Zhong performed the electrocatalytic reaction studies and analyzed the data. Xu Lu and Hailiang Wang wrote the paper. Yongye Liang, Neil B. McKeown and Hailiang Wang supervised the project.

## Appendix A. Supplementary data

Supplementary data to this article can be found online at https://doi.org/10.1016/j.scib.2019.04.008.

## References

[1] Li J, Chen G, Zhu Y, et al. Efficient electrocatalytic $CO_2$ reduction on a three-phase interface. Nat Catal 2018;1:592–600.
[2] Rasul S, Anjum DH, Jedidi A, et al. A highly selective copper-indium bimetallic electrocatalyst for the electrochemical reduction of aqueous $CO_2$ to CO. Angew Chem Int Ed 2015;54:2146–50.
[3] Liu M, Pang Y, Zhang B, et al. Enhanced electrocatalytic $CO_2$ reduction via field-induced reagent concentration. Nature 2016;537:382.
[4] Kim D, Sakimoto KK, Hong D, et al. Artificial photosynthesis for sustainable fuel and chemical production. Angew Chem Int Ed 2015;54:3259–66.
[5] Lu Q, Rosen J, Zhou Y, et al. A selective and efficient electrocatalyst for carbon dioxide reduction. Nat Commun 2014;5:3242.
[6] Reske R, Mistry H, Behafarid F, et al. Particle size effects in the catalytic electroreduction of $CO_2$ on Cu nanoparticles. J Am Chem Soc 2014;136:6978–86.
[7] Singh MR, Clark EL, Bell AT. Effects of electrolyte, catalyst, and membrane composition and operating conditions on the performance of solar-driven

electrochemical reduction of carbon dioxide. Phys Chem Chem Phys 2015;17:18924–36.

[8] Whipple DT, Kenis PJ. Prospects of $CO_2$ utilization via direct heterogeneous electrochemical reduction. J Phys Chem Lett 2010;1:3451–8.

[9] Roy S, Sharma B, Pécaut J, et al. Molecular cobalt complexes with pendant amines for selective electrocatalytic reduction of carbon dioxide to formic acid. J Am Chem Soc 2017;139:3685–96.

[10] Kortlever R, Shen J, Schouten KJP, et al. Catalysts and reaction pathways for the electrochemical reduction of carbon dioxide. J Phys Chem Lett 2015;6:4073–82.

[11] Zumdahl SS. Chemical principles. 5th ed. Boston, NY: Houghton Mifflin College Division; 2005.

[12] Wang T, Lackner KS, Wright AB. Moisture-swing sorption for carbon dioxide capture from ambient air: a thermodynamic analysis. Phys Chem Chem Phys 2013;15:504–14.

[13] Li H, Wilhelmsen Ø, Yan J. Properties of $CO_2$ mixtures and impacts on carbon capture and storage. In: Handbook of clean energy systems. Hoboken, NJ: John Wiley & Sons, Ltd.; 2015. p. 1–17.

[14] Stamenkovic VR, Fowler B, Mun BS, et al. Improved oxygen reduction activity on $Pt_3Ni$ (111) via increased surface site availability. Science 2007;315:493–7.

[15] Chen Y, Li CW, Kanan MW. Aqueous $CO_2$ reduction at very low overpotential on oxide-derived Au nanoparticles. J Am Chem Soc 2012;134:19969–72.

[16] Yu KMK, Curcic I, Gabriel J, et al. Recent advances in $CO_2$ capture and utilization. ChemSusChem 2008;1:893–9.

[17] Aaron D, Tsouris C. Separation of $CO_2$ from flue gas: a review. Sep Sci Technol 2005;40:321–48.

[18] Price GD, Badger MR, Woodger FJ, et al. Advances in understanding the cyanobacterial $CO_2$-concentrating-mechanism (CCM): functional components, Ci transporters, diversity, genetic regulation and prospects for engineering into plants. J Exp Botany 2007;59:1441–61.

[19] Rakowski Dubois M, Dubois DL. Development of molecular electrocatalysts for $CO_2$ reduction and H2 production/oxidation. Acc Chem Res 2009;42:1974–82.

[20] Kozaki A, Takeba G. Photorespiration protects C3 plants from photooxidation. Nature 1996;384:557.

[21] Kim SJ, Matsumoto M, Shigehara K. Synthesis and electrical properties of one-dimensional octacyanometallophthalocyanine (M≡Fe, Co) polymers. J Porphyr Phthalocya 2000;4:136–44.

[22] Zhang X, Wu Z, Zhang X, et al. Highly selective and active $CO_2$ reduction electrocatalysts based on cobalt phthalocyanine/carbon nanotube hybrid structures. Nat Commun 2017;8:14675.

[23] Wu Z, Gan Q, Li X, et al. Elucidating surface restructuring-induced catalytic reactivity of cobalt phosphide nanoparticles under electrochemical conditions. J Phys Chem C 2018;122:2848–53.

[24] Budd PM, Msayib KJ, Tattershall CE, et al. Gas separation membranes from polymers of intrinsic microporosity. J Membr Sci 2005;251:263–9.

[25] Lu X, Wu Y, Yuan X, et al. High performance electrochemical $CO_2$ reduction cells based on non-noble metal catalysts. ACS Energy Lett 2018;3:2527–32.

[26] Weng Z, Jiang J, Wu Y, et al. Electrochemical $CO_2$ reduction to hydrocarbons on a heterogeneous molecular Cu catalyst in aqueous solution. J Am Chem Soc 2016;138:8076–9.

[27] Li CW, Ciston J, Kanan MW. Electroreduction of carbon monoxide to liquid fuel on oxide-derived nanocrystalline copper. Nature 2014;508:504.

[28] Jouny M, Luc W, Jiao F. High-rate electroreduction of carbon monoxide to multi-carbon products. Nat Catal 2018;1:748–55.

[29] Spurgeon JM, Kumar B. A comparative technoeconomic analysis of pathways for commercial electrochemical $CO_2$ reduction to liquid products. Energy Environ Sci 2018;11:1536–51.

[30] Fang Y, Flake JC. Electrochemical reduction of $CO_2$ at functionalized Au electrodes. J Am Chem Soc 2017;139:3399–405.

[31] Zhao S, Jin R, Jin R. Opportunities and challenges in $CO_2$ reduction by gold-and silver-based electrocatalysts: from bulk metals to nanoparticles and atomically precise nanoclusters. ACS Energy Lett 2018;3:452–62.

[32] Kornienko N, Zhao Y, Kley CS, et al. Metal-organic frameworks for electrocatalytic reduction of carbon dioxide. J Am Chem Soc 2015;137:14129–35.

[33] Costentin C, Drouet S, Robert M, et al. A local proton source enhances $CO_2$ electroreduction to CO by a molecular Fe catalyst. Science 2012;338:90–4.

[34] Carta M, Malpass Evans R, Croad M, et al. An efficient polymer molecular sieve for membrane gas separations. Science 2013;339:303–7.

[35] Carrott P, Cansado I, Carrott MR. Carbon molecular sieves from PET for separations involving $CH_4$, $CO_2$, $O_2$ and $N_2$. Appl Surface Sci 2006;252:5948–52.

[36] Walker Jr PL, Mahajan OP. Pore structure in coals. Energy Fuels 1993;7:559–60.

[37] Li S, Falconer JL, Noble RD. Improved SAPO-34 membranes for $CO_2/CH_4$ separations. Adv Mater 2006;18:2601–3.

Xu Lu obtained his B.S. and Ph.D. degrees from University of Hong Kong in 2012 and 2017, respectively. He is currently a postdoctoral associate in the Department of Chemistry, Yale University under the supervision of Prof. Hailiang Wang. His research focuses on reactor engineering and applications in energy conversion and storage.

Yongye Liang received his Ph.D. degree from University of Chicago in 2009. He is currently Professor of Materials Science and Engineering at Southern University of Science and Technology, China. His research focuses on the development of advanced materials for energy, electronics and biotechnology through the combination of chemical design and synthesis with device studies.

Neil B. McKeown is currently the Crawford Tercentenary Chair of Chemistry and Director of Research, School of Chemistry, University of Edinburgh. His research interests cover synthesis of organic materials, polymers of intrinsic microporosity, membranes, $CO_2$ capture, and nanoporous molecular crystals.

Hailiang Wang received his Ph.D. degree from Stanford University in 2012. He is currently Assistant Professor of Chemistry at Yale University. His research group strives to understand material structures and properties at the solid/liquid interface under electrochemical conditions and to establish design principles for new and improved electrocatalysts and battery materials for reactions related to the development of alternative energy sources.